Modulation depth effects in photorefractive two-wave mixing

F. Pauly[1], O. Sandfuchs[2], F. Kaiser[3], M. Belić[4]

[1] *Institute for Theoretical Solid State Physics, Karlsruhe University, 76128 Karlsruhe, Germany*

[2] *Carl Zeiss Jena GmbH, 07745 Jena, Germany*

[3] *Institute of Applied Physics, Darmstadt University of Technology, Germany*

[4] *Texas A&M University at Qatar, Doha, Qatar*

High modulation depth effects in contra-directional two-wave mixing in photorefractive crystals are investigated. A modified two-wave mixing model is used that includes a correction function for the high modulation depth. Transverse instabilities arise when the modulation depth at one side of the crystal is close to unity, hence high modulation depth effects must be taken into account. In the near field transverse running waves appear above the instability threshold. A physical justification for the correction function is presented, by analyzing Kukhtarev's material equations. For static gratings a real and superlinear correction function is found, whereas for running gratings a complex correction function with a sublinear real part is obtained.

1. Introduction

A while ago Kukhtarev et al. [1] developed a band transport model that describes the response of a photorefractive (PR) crystal to a light distribution. According to the model an interference pattern in the crystal builds up a space charge field that induces a refractive index modulation, thanks to the linear Pockels effect. A treatable system of differential equations is obtained by use of simplifying assumptions. One such assumption is the low modulation depth m of the interference pattern [2]. To extend the validity of two-wave mixing (TWM) equations to the regime of high modulation depths, introduction of a correction function $f(m)$ has been suggested by Refregier et al. [3]. Thus far a number of such functions $f(m)$ has been proposed, based either on the analysis of Kukhtarev's equations (KE) or on experimental findings [4-9]. Examples include $f(m) = (1 - e^{-am})/a$ [3] and $f(m) = m/(1 + bm)$ [4], while $f(m) = m$ represents the small-m limit [2].

In recent years instabilities in contra-directional TWM attracted considerable attention. Since the observation of hexagonal patterns in the far field of a feedback configuration [10, 11], many additional structures, such as stripes and squares, have been found [12, 13]. With the help of linear stability analysis a better understanding of these structures is achieved [14-17]. However, high modulation depth effects have mostly been ignored. An exemption is our own paper [18]. The present contribution brings a simplified version of our theory and results.

The paper is divided in two parts. In the first part the spatiotemporal pattern formation in contra-directional TWM is investigated numerically, with the inclusion of high modulation depth. A sublinear correction function $f(m) = m/(1 + bm)$ with the saturation $b \geq 0$, as proposed by Kwak et al. [4], is used for this purpose. While this function is not appropriate for static gratings – and this is substantiated in the paper – it is well suited for introducing nonlinear response into TWM, and for accounting high modulation depth effects. Furthermore, it can display a superlinear behavior, provided one allows for negative values of b. We also demonstrate that in the contra-directional TWM the modulation depth at one face of the crystal is near unity at the instability threshold.

In the second part of the paper the foundation of high modulation depth corrections, based on the underlying material KE [18-27], is discussed. We investigate numerical solutions of the band transport model with a spectral integration scheme. The space charge field is computed for stationary intensity patterns, with and without applied electric field, as well as for moving patterns. We show that with the correct consideration of the phases of interacting beams a superlinear real correction function has to be used for the static case, whereas a complex valued correction function is necessary for the moving interference fringes.

2. Pattern formation with high modulation depth

Contra-directional TWM in one transverse dimension is described by the equations [17]:

$$\partial_z A_1 + \mathrm{i} f \partial_x^2 A_1 = -Q A_2 \,, \tag{1}$$

$$-\partial_z A_2 + \mathrm{i} f \partial_x^2 A_2 = Q^* A_1 \,, \tag{2}$$

$$\tau \partial_t Q + \eta Q = \frac{\Gamma}{2} f(m) e^{\mathrm{i}(\psi_1 - \psi_2)} \,. \tag{3}$$

In Eq. (3) the modulation depth m is replaced by the correction function $f(m)$.

The propagation of two counter-propagating beams in a PR medium (Fig. 1) is described by Eqs. (1) and (2). $A_i(x, z, t)$ are the slowly-varying envelopes of the light fields. The parameter $f = L/\left(2 k_0 w_0^2\right)$ is proportional to the inverse of the Fresnel number. L is the length of the crystal and k_0 the wave vector of beams in the crystal along the propagation (z) direction. The transverse coordinate is scaled to the beam waist w_0. The beams couple through the grating amplitude Q, given by

$$Q = -\mathrm{i} L k_0 n_0^2 r_{\mathrm{eff}} E_1^{\mathrm{sc}}/4 \,, \tag{4}$$

where n_0 is the ordinary refractive index of the crystal, r_{eff} the effective electro-optical coefficient and E_1^{sc} stands for the first Fourier component of the space charge field. The beam coupling arises through a periodic refractive index variation with the grating wave vector $K_{\mathrm{g}} = 2 k_0$.

Equation (3) describes the temporal evolution of E_1^{sc}. It is derived from KE. The derivation is carried out by assuming a small fringe contrast of the interference pattern, characterized by the modulation depth

$$m = \frac{2 |A_1| |A_2|}{|A_1|^2 + |A_2|^2} \,. \tag{5}$$

In this manner KE are linearized, and all higher harmonics are neglected. Furthermore, the transverse spatial derivatives of the Fourier components are ignored, assuming that the crystal's internal properties depend only on z.

The variables ψ_i ($i = 1, 2$) in Eq. (3) are the phases of the beam envelopes $A_i = |A_i| \exp(\mathrm{i}\psi_i)$ and τ stands for the characteristic PR response time. The coupling constant Γ is given by

$$\Gamma = \Gamma_0 \left(1 + \frac{E_{\mathrm{q}}}{E_{\mathrm{d}}}\right) \frac{E_{\mathrm{d}} + \mathrm{i} E_0}{E_{\mathrm{q}} + E_\mu + \mathrm{i} E_0} \tag{6}$$

and the relaxation constant by

$$\eta = \frac{(E_{\mathrm{d}} + E_{\mathrm{q}} + \mathrm{i} E_0)}{(E_{\mathrm{d}} + E_\mu + \mathrm{i} E_0)} \,. \tag{7}$$

The parameters η and Γ depend on an externally applied electric field E_0 (see Fig. 1). The fields E_{d}, E_μ and E_{q}, respectively the diffusion field, the drift field and the limiting space charge field, are the characteristic fields of the crystal. In the TWM simulations these fields are chosen to be $E_{\mathrm{d}} = 1\mathrm{kV/cm}$, $E_\mu = 100 E_{\mathrm{d}}$ and $E_{\mathrm{q}} = 5 E_{\mathrm{d}}$, describing a BaTiO$_3$ crystal. Γ_0 is set to 2 and f to 0.025.

The boundary conditions in contra-directional TWM consist of the fixed beam profiles at $z = 0$ for the beam one and at $z = L$ for the beam two. For TWM simulations we use Gaussian beams incident upon opposite faces of the crystal

$$A_1(x, z = 0) = |A_1(x = 0, z = 0)| e^{-x^2/w_0^2} \,, \tag{8}$$

$$A_2(x, z = L) = |A_2(x = 0, z = L)| e^{-x^2/w_0^2} \,. \tag{9}$$

Since only relative intensities play a role in the model, we define the beam ratio r as

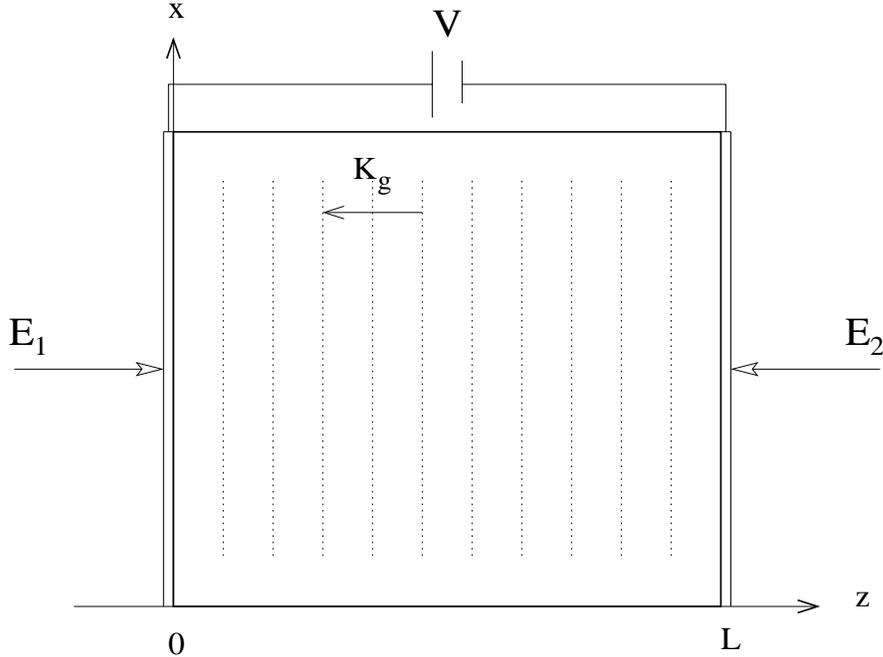$$r := \frac{I_1(x = 0, z = 0)}{I_2(x = 0, z = L)} \,, \tag{10}$$

Figure 1: Geometry of wave mixing. Two beams E_1 and E_2 are propagating in the opposite directions in a photorefractive crystal. The externally applied electric field $E_0 = V/L$ is adjusted by an external voltage V.

and set $|A_1 (x = 0, z = 0)| = 1$ and $|A_2 (x = 0, z = L)| = (r)^{-1/2}$.

In our TWM simulations we integrate the full set of Eqs. (1)-(3) for incident Gaussian beams, using the method of Ref. [17]. The longitudinal behavior of the modulation depth $m (x = 0, z)$, as obtained for Gaussian beams, is represented in Fig. 2. It is seen that the modulation depth in the region of $z = 0$ is high, being nearly one for all beam ratios and saturations b. This is recognized as a characteristic of an instability threshold. The case $r = 25$ is quite close to the constant modulation depth $m = 1$, because for this beam ratio the modulation depth is hardly departing from unity within the crystal. However, the modulation depth is generally not constant over the whole range of the crystal, but decreases monotonically with increasing z. At the instability threshold the longitudinal behavior of the modulation depth is nearly the same for different saturations b, which is achieved by an adjustment of E_0. For different beam ratios the curve shape of the modulation depth varies considerably, and it is decaying faster towards the crystal's end for high r. Thus, for high intensity ratios there is a significant departure from $m (z) = 1$.

In the determination of critical quantities using simulations it is a general problem that, because of the finite modulations observed above the threshold, the instability boundary can only be approximated. Critical quantities, such as the transverse wave vector and the oscillation frequency, are thus identified slightly above the threshold. The discrepancies between the simulations and analytical results are the consequence of using Gaussian beams, in comparison to the stability analysis with plane waves. Only at high aspect ratios, i.e. at high numbers of transverse modulations across broad Gaussian beam profile, the results should be the same. Under these conditions, the predictions of the stability analysis match the values obtained from the simulations.

Below the instability threshold of the TWM simulations the system converges to a temporally stationary state. The beams are counter-propagating and the signal beam is amplified by the pump beam. Above the threshold transverse running waves appear in the near field at either side of the crystal (Fig. 3). From the excitation source in the middle of the beams, the waves are moving outwards atop the Gaussian carrier wave. The structures behave temporally periodic and this behavior is changed neither by different intensity ratios r nor by different saturations b. Compared to the situation shown in Figs. 3 (a) and (b) for $b = 1.5$, $r = 250$
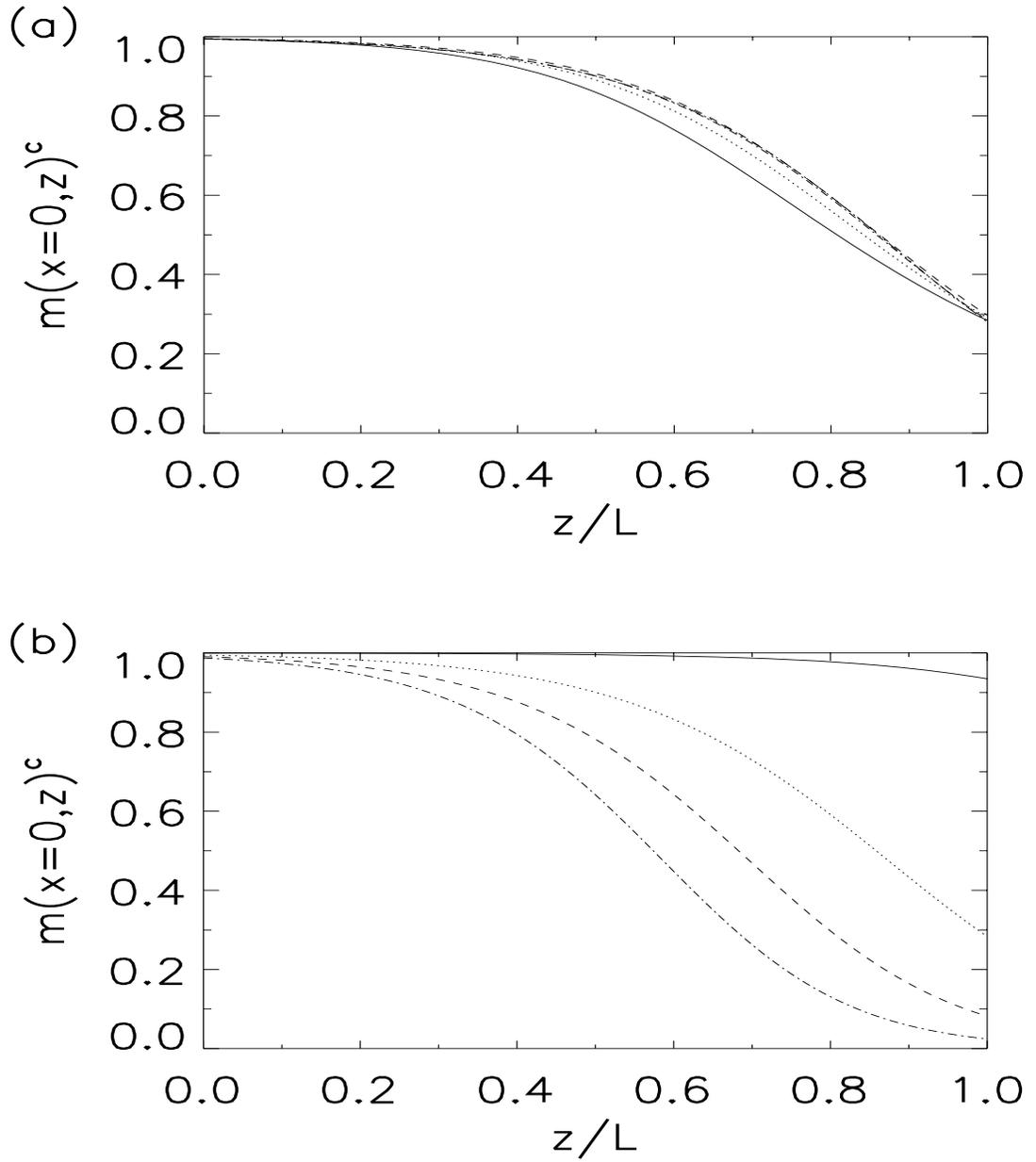
Figure 2: Longitudinal behavior of the critical modulation depth $m\,(x=0,z)^{\mathrm{c}}$ for different saturations b and intensity ratios r as obtained from numerical simulations with Gaussian beams. (a): (——) $b=0$, (······) $b=0.5$, (- - - -) $b=1$, (-·-·-·) $b=1.5$, (-··-··-) $b=2$ and $r=250$, respectively, (b): (——) $r=25$, (······) $r=250$, (- - - -) $r=2500$, (-··-··-) $r=2.5\times10^4$ and $b=1.5$, respectively.
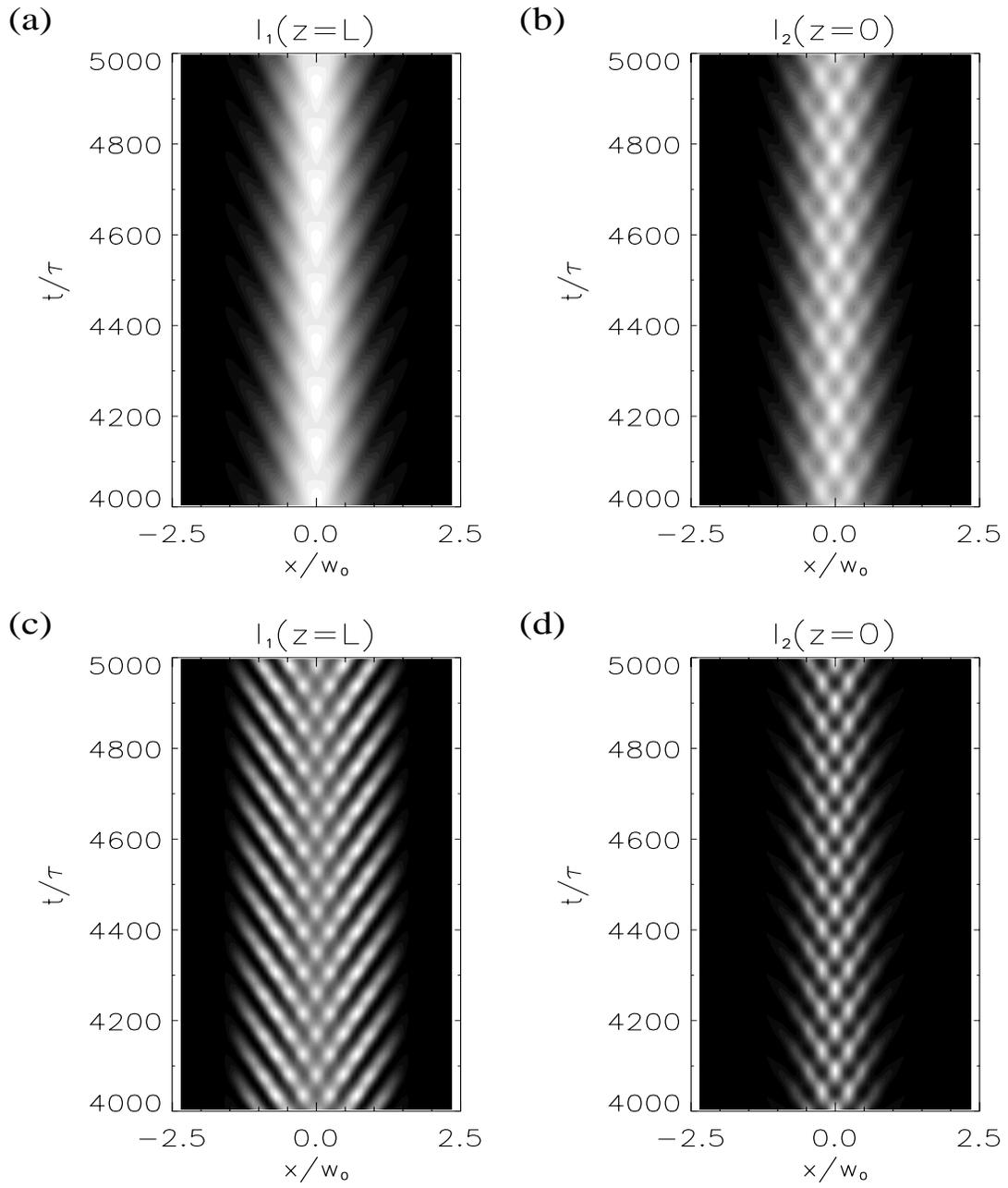
Figure 3: Transverse running waves in the near field: $I_1\,(x, z = L)$ and $I_2\,(x, z = 0)$ for $b = 1.5$, $r = 250$ and (a)-(b) $E_0 = -7.0E_\mathrm{d}$, (c)-(d) $E_0 = -8.5E_\mathrm{d}$.

and $E_0 = -7.0E_\mathrm{d}$, the external field strength is increased to $E_0 = -8.5E_\mathrm{d}$ in Figs. 3 (c) and (d). Owing to the higher magnitude of the applied field, the amplitudes of the transverse modulations are strongly enhanced and the oscillation frequency is increased. The stronger modulations signify a stronger energy transfer to the side-band beams, which can be observed in the optical far field after a Fourier transformation of the complex envelopes. Two temporally changing peaks at the critical wave numbers $\pm K^\mathrm{c}$ appear in the far field around the zeroth order, corresponding to the Fourier transform of the Gaussian beam.

Summarizing our TWM simulations in the broad parameter range of variable saturation b, beam ratio r and field strength E_0, there exists a region where periodic spatio-temporal patterns are observed above the instability threshold. Depending on the intensity ratio r and the saturation b, this region extends over a field strength interval of $\Delta E_0 = 1E_\mathrm{d}$ at low b and high r, or $\Delta E_0 = 5E_\mathrm{d}$ at low b and low r. At higher b these regions are even broader. A change of both the beam ratio in the region of $r = 25$ to 10^5 and the saturation from $b = 0$ to 2 does not have any qualitative influence on the running transverse waves.

Concerning applications of TWM, the signal beam amplification g_S is one of the interesting physical quantities. It is defined as

$$g_\mathrm{S} := \left\langle \left(\int_{-\infty}^{\infty} \mathrm{d}x I_2 \left(x, z = 0 \right) \right) / \int_{-\infty}^{\infty} \mathrm{d}x I_2 \left(x, z = L \right) \right\rangle_t \tag{11}$$

and is equal to the ratio of the total outgoing to the total incoming energy of the signal beam. Analogously, the gain g_P of the pump beam is defined as

$$g_\mathrm{P} = \left\langle \left(\int_{-\infty}^{\infty} \mathrm{d}x I_1 \left(x, z = L \right) \right) / \int_{-\infty}^{\infty} \mathrm{d}x I_1 \left(x, z = 0 \right) \right\rangle_t . \tag{12}$$

This property measures the energy transfer to the signal beam. Because a modulation depth close to unity has been recognized as the characteristic of the instability threshold for plane waves, as well as for Gaussian beams, the critical gain is qualitatively in the order of the intensity ratio r.

In Fig. 4 the gain values of the pump and signal beam, determined by simulations of Gaussian beams, are compared to the ones for stationary plane waves. Below the numerically identified critical field strength, the gain values for Gaussian beams coincide with the calculations for plane waves. Above the threshold, however, a saturation of the gain g_S is observed (Figs. 4 (a) and (c)). The results for other parameters are identical. The gain of the pump beam g_P behaves analogously and exhibits a very good agreement between the simulations and semi-analytical values below E_0^c and a departure from the plane-wave predictions above the instability threshold (Figs. 4 (b) and (d)). These results are consistent with the requirement of energy conservation. Above the onset of transverse instabilities, the signal beam is no more amplified, as indicated by the saturating gain g_S. The additional energy is now available for the pump beam, and the gain of the pump beam g_P does not decrease any more. For applications this result implies that, within the confines of the model, signal amplification can only occur up to the critical field strength, beyond which instabilities and pattern formation prevent energy transfer to the signal beam.

3. Foundation of high modulation depth corrections

Even though the correction function $f\left(m\right)$ is introduced on phenomenological grounds, we attempt to provide a better insight into its physical foundation. To this end we discuss nonlinear response of the first Fourier component of the space charge field E_1^sc, based on the underlying KE. For this purpose the TWM process is decoupled and it is assumed that the crystal is exposed to a certain intensity pattern. Then the response of the crystal is determined. This response does not influence the intensity pattern in turn. Numerical solutions of KE are computed, placing the emphasis on the buildup of the space charge field. By a Fourier transformation of the electric field in the crystal, the behavior of the relevant TWM quantity E_1^sc is extracted, which is responsible for the beam coupling in our model.

The response of a PR crystal exposed to a laser light is described by Kukhtarev's band transport model
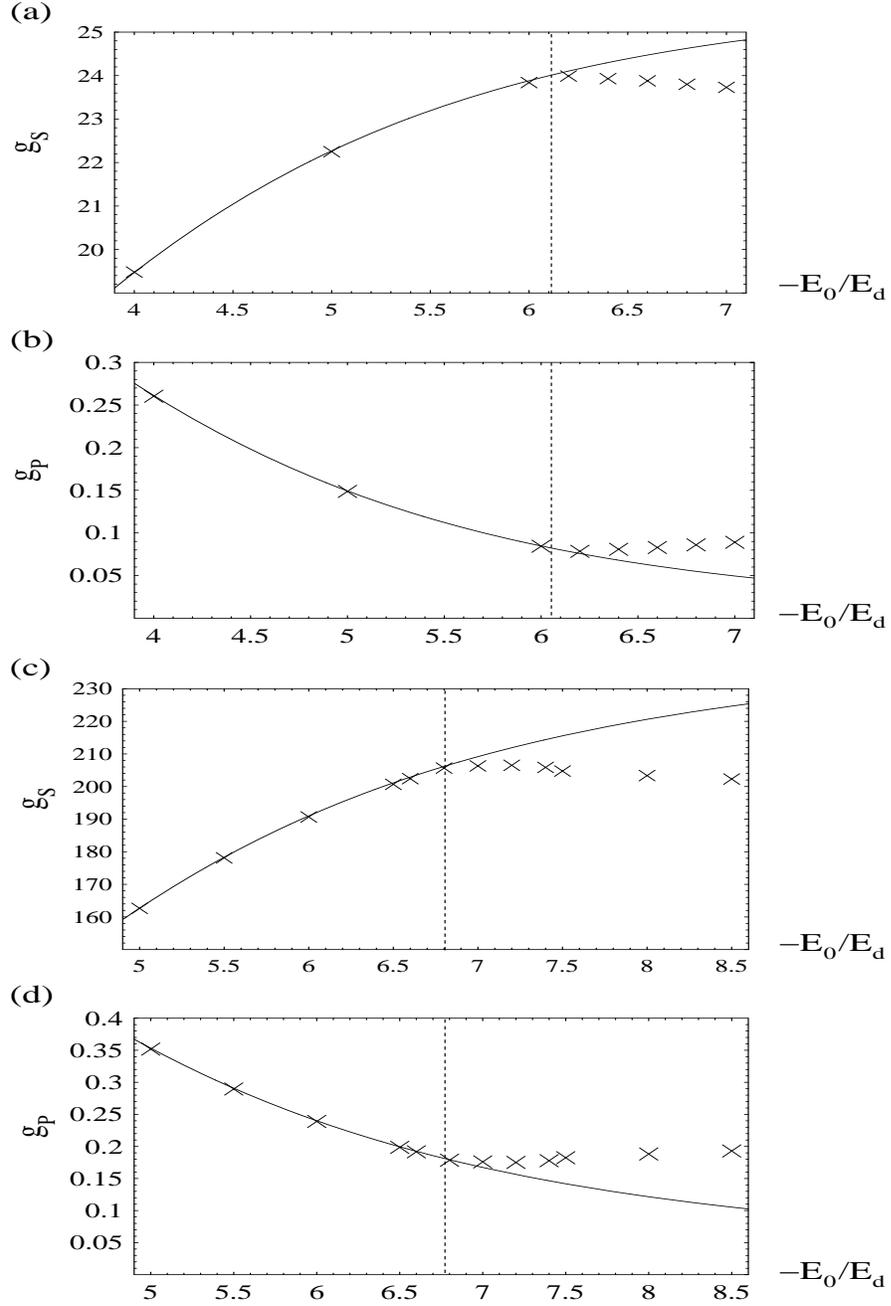
(a)

(b)

(c)

(d)

Figure 4: Gain of the signal and the pump beam g_S and g_P as functions of the field strength for $b = 1.5$ and $r = 25$ ((a) and (b)) as well as for $r = 250$ ((c) and (d)). The numerically determined critical field strength is indicated by a vertical line. ($\times$): results for Gaussian beams, (——) results for plane waves using the method of Belić [7].

[2]:

$$\partial_t N_\mathrm{D}^+ = (sI + \beta_\mathrm{th})\left(N_\mathrm{D} - N_\mathrm{D}^+\right) - \gamma_\mathrm{R} N N_\mathrm{D}^+ , \tag{13}$$

$$\partial_t N - \partial_t N_\mathrm{D}^+ = \frac{1}{e}\vec{\nabla}\cdot\vec{j} , \tag{14}$$

$$\vec{j} = \mu\left(eN\vec{E} + k_\mathrm{B}T\vec{\nabla}N\right) , \tag{15}$$

$$\vec{\nabla}\cdot\varepsilon\vec{E} = \rho = e\left(N_\mathrm{D}^+ - N_\mathrm{A}^- - N\right) , \tag{16}$$

where N is the electron density, N_A^- and N_D^+ are the densities of ionized acceptors and donors, $\vec{j}$ is the current density, $\vec{E}$ is the electric field in the crystal, ρ is the charge density, I is the light intensity, s is the cross section of photo ionization, β_th the thermal excitation rate, γ_R the recombination constant, $e = |e|$ the (positive) electron charge, μ the mobility, k_B Boltzmann's constant, T the temperature, and ε the dielectric constant. Equations (13)-(16) – the KE – are treated numerically, and we restrict ourselves to one spatial dimension. This dimension is the longitudinal z-direction, because E_1^sc is the Fourier component of the space charge field along the grating wave vector $\vec{K}_\mathrm{g}$. All quantities are thus scalar and the spatial gradient is replaced by the derivative $\vec{\nabla} \to \partial_z$.

The crystal is assumed to be exposed to an intensity pattern, which is uniform in x and y, with a cosinusoidal profile infinitely extended in the z-direction. Under such conditions all other quantities of the crystal are periodic functions, with the period Λ of the intensity pattern. To reduce computational efforts, it is sufficient to solve Eqs. (13)-(16) under periodic boundary conditions on an interval of the length Λ. This length is approximately $2 \times \lambda = 1\mu$m for visible light of wave length $\lambda \approx 500$nm, when the intensity pattern arises from the interference of two counter-propagating beams. However, by tilting the beams, this length Λ can be increased, and for the simulations a value of $\Lambda = \lambda/\cos\gamma = 10\mu$m has been chosen, based on Ref. [19]. In this reference a finitely-extended super-Gaussian intensity distribution, multiplied by a periodic modulation, has been investigated in one dimension, leading to a relatively broad spatial region of periodic response. This justifies our assumption of periodic boundaries, already employed in Ref. [20].

The system of Eqs. (13)-(16) is integrated by the method described in Ref. [18]. The initial values are chosen such that the light is switched on at $t = 0$. For $t < 0$ the intensity is therefore $I = 0$, and the crystal is in a stationary, spatially homogeneous state. For $t > 0$ a light field is present in the crystal, with the following intensity distribution

$$I(z,t) = I_0\left[1 + m\cos\left(2\pi z - \varpi t\right)\right] . \tag{17}$$

In the case of $\varpi = 0$, Eq. (17) represents static gratings, otherwise running gratings. The crystal parameters are chosen according to Ref. [19] and are based on experimental data describing a $\mathrm{Bi}_{12}\mathrm{SiO}_{20}$ crystal (BSO): $N_\mathrm{D} = 10^{25}\mathrm{m}^{-3}$, $N_\mathrm{A} = 0.95 \times 10^{22}\mathrm{m}^{-3}$, $\mu = 10^{-5}\mathrm{m}^2/\mathrm{Vs}$, $\gamma_\mathrm{R} = 1.65 \times 10^{-17}\mathrm{m}^3\mathrm{s}^{-1}$, $s = 1.06 \times 10^{-5}\mathrm{m}^2/\mathrm{J}$ and $\varepsilon = 9.7\varepsilon_0$.

We remark that the parameters of the BSO crystal used in this part differ from the BaTiO_3 crystal discussed in the first part. This is for reasons of comparison, because up to now most of the simulations on running gratings have been performed for BSO crystals [8, 20]. The internal fields of the BSO crystal are: $E_\mathrm{d} = k_\mathrm{B}TK_\mathrm{g}/e = 1.59 \times 10^4\mathrm{V/m}$, $E_\mathrm{q} = eN_\mathrm{A}/(\epsilon K_\mathrm{g}) = 2.82 \times 10^7\mathrm{V/m} \approx 1.77 \times 10^3 E_\mathrm{d}$ and $E_\mu = \gamma_\mathrm{R}N_\mathrm{A}/(\mu K_\mathrm{g}) = 2.49 \times 10^4\mathrm{V/m} \approx 1.57E_\mathrm{d}$.

The length of the intensity period is set to $\Lambda = 10\mu$m (as mentioned), and the intensity of the incident laser radiation to $I_0 = 10^4\mathrm{W/m}^2$. The effective intensity contrast in the PR crystal is reduced by thermal effects. To investigate the influence of high modulation depth, a negligible thermal excitation rate ($\beta_\mathrm{th} = 0$) is assumed. In the following we investigate both stationary and running intensity distributions at room temperature ($T = 293$K). The applied field E_0 is varied between 0 and $5 \times 10^4\mathrm{V/m}$, and the modulation depth of the intensity profiles, present in the crystal, is altered from $m = 0$ to $m = 1$ Stationary intensity distribution is depicted in Fig. 5.

In Fig. 6 the electric field in the crystal is shown for the stationary intensity distributions given in Fig. 5, under the influence of different externally applied fields E_0. Results for the maximum modulation depth
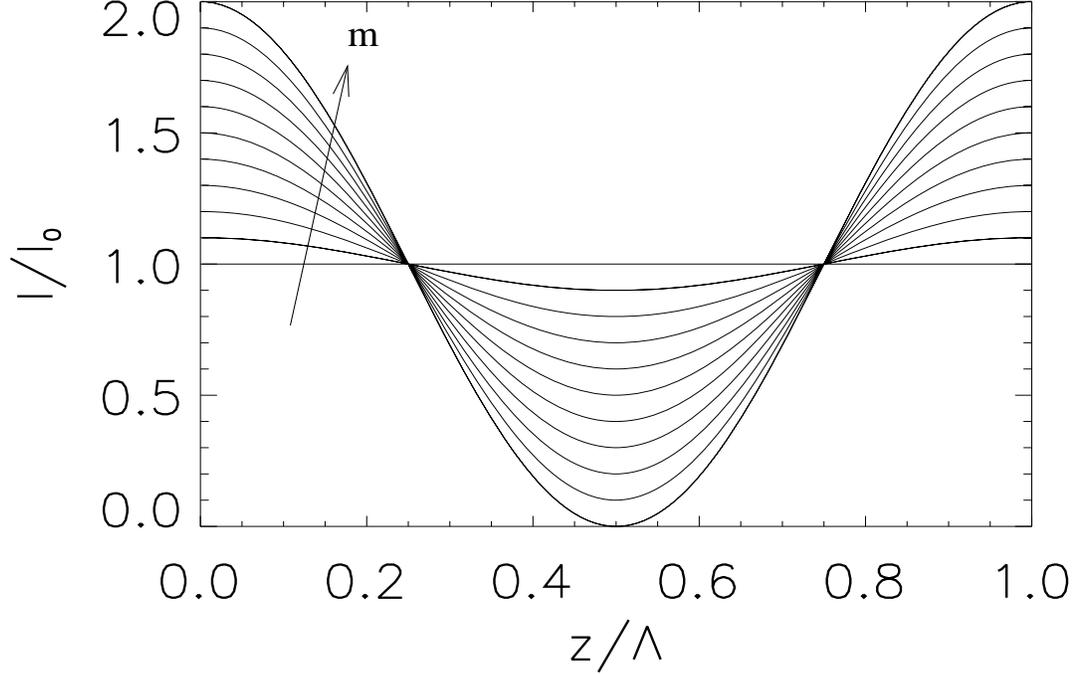
Figure 5: Stationary intensity distributions present in the crystal for $m = 0$, 0.1, ..., 1. The modulation depth is increasing in the direction indicated by the arrow.

$m = 1$ are not depicted, because the convergence is slow and transients persist for very long. According to KE, the field E represents the total electric field in the crystal, $E = E^{sc} + E_0$.

For small modulation depth ($m = 0.1$ and 0.2), and without an externally applied field (Fig. 6 (a)), a sinusoidal electric field is obtained as a response to the cosinusoidal intensity distribution. These solutions correspond to the approximate small-m solutions given in Refs. [1, 2]. For higher modulation depth a strongly nonlinear response is observed. The gradients at $z = 0.5$ become gradually steeper, preventing the diffusion of charge carriers into the dark region. The sign of the space charge field switches at the minimum of the intensity ($z = 0.5$), to oppose the diffusion by drift forces. The first Fourier component of the space charge field is purely imaginary, owing to the point symmetry around $z = 0.5$.

In Figs. 6 (b) and (c) an external field, pointing into the positive z-direction, is applied to the crystal. It can clearly be seen how the external field destroys the point symmetry around $z = 0.5$. In Fig. 6 (b) a phase shift of the space charge field develops, compared to Fig. 6 (a), as well as an asymmetry between the maximum and minimum value of E, which is not simply due to the bias $E_0 = 0.31E_d$. Because of the phase shift, the first Fourier component of the space charge field is no more purely imaginary. This effect is contained in the E_0-dependent coefficients η and Γ in Eq. (3). The higher field strength $E_0 = 3.1E_d$ (Fig. 6 (c)) has brought us to the drift-dominated regime, in contrary to the diffusion-dominated regime in Fig. 6 (a). In Fig. 6 (c) the electric field resembles a negative cosine curve for small modulation depths, similar to the analytical approximate solutions presented in Ref. [24] for the case without diffusion. The phase shift between the interference pattern and the space charge field is almost π. As already observed in Figs. 6 (a) and (b), the spectra of E reveal high amplitudes of the higher harmonic terms, especially for $m = 0.9$. The trends visible in Fig. 6 (b) are much more pronounced in Fig. 6 (c). The maximum of the space charge field has
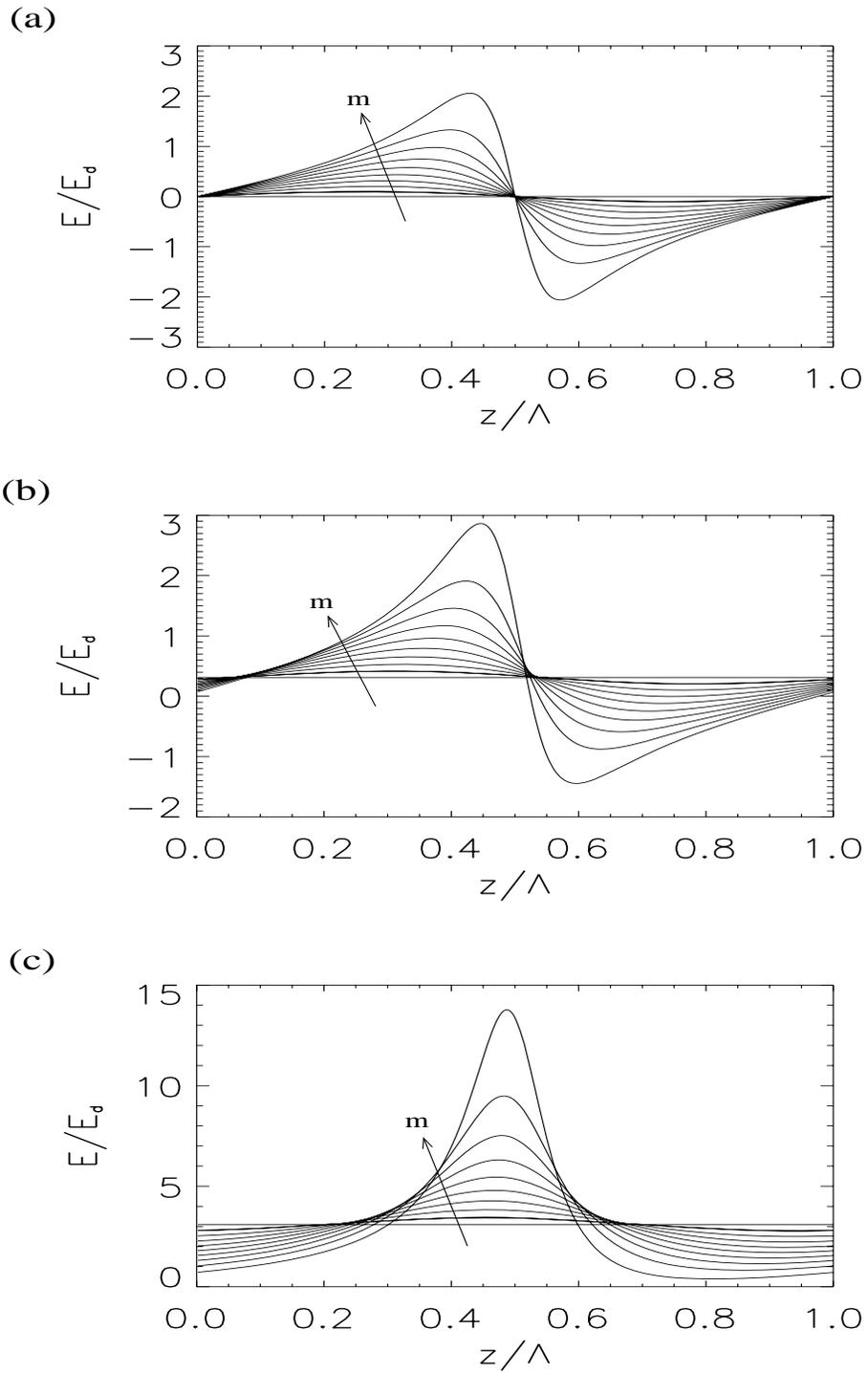
(a)

(b)

(c)

Figure 6: The total electric field in the crystal $E = E_0 + E^{\mathrm{sc}}$ for different applied external fields: (a) $E_0 = 0$, (b) $E_0 = 0.31E_{\mathrm{d}}$, (c) $E_0 = 3.1E_{\mathrm{d}}$. The modulation depth is varied from $m = 0$ to $m = 0.9$ in steps of $\Delta m = 0.1$. The direction of increasing m is indicated by the arrow.

strongly grown for high m and is shifted to the right, which is due to the higher field E_0, pulling the electrons to the right of the symmetry point $z = 0.5$. The minimum in the field strength to the right of $z = 0.5$ is washed out, and the asymmetry between values below the bias field E_0 and above is apparent. These effects are observable, especially for a high modulation depth, and evidently are caused by the nonlinear character of KE.

Other internal crystal quantities, as for example the electron density and the ionized donor density, are not represented here. Interestingly – as reported in Refs. [22, 25] – a nearly perfect cosinusoidal response of the excited electron density is observed for different modulation depths m and even for different externally applied fields E_0. This, in a way, runs against the first intuition, that the applied E_0 should break the symmetry around $z = 0.5$ in all crystal's internal variables. However, it turns out that the excited electron density simply "copies" the intensity distribution, and the second harmonics are already orders of magnitude smaller than the first Fourier components.

The response of the crystal to running intensity distributions is given by Eq. (17) with $\varpi \neq 0$. The term $\exp\left[\mathrm{i}\left(\psi_1 - \psi_2\right)\right]$ in Eq. (3) is replaced by $\exp\left(-\mathrm{i}\delta\omega t\right)$, which acts as an oscillatory forcing term. This time dependence arises because the phase difference $\psi_1 - \psi_2$ in Eq. (3) is equal to $-\delta\omega t$, owing to the special form of the intensity pattern in Eq. (17). If the imaginary part of η is at the same frequency as the forcing term, a resonance phenomenon can be expected (provided the real part of η is small), leading to a high first-order harmonic that should strengthen the interaction between the counter-propagating beams in a TWM experiment. Carrying out the calculations, as described in Ref. [3], and scaling with the recombination time $\tau_{\mathrm{R}} = \left(\gamma_{\mathrm{R}} N_{\mathrm{A}}\right)^{-1}$, yields an optimum value of the frequency detuning $\varpi_{\mathrm{opt}} \approx 0.24$. Another possibility to compute the frequency at which the first Fourier component takes maximum value, is to decompose all crystal's internal quantities in terms of $\exp\left(\pm\mathrm{i}\left(2\pi z - \varpi t\right)\right)$. Using Eq. (21) from Ref. [3] one obtains $\varpi_{\mathrm{opt}} \approx 0.28$.

Henceforth, the simulations with running gratings are carried out with $\varpi = 0.25$. A high amplitude of the first Fourier component of the induced space charge field is expected for this frequency, as is visible in Fig. 7. The space charge field resembles a sine function for small m, similar to the diffusion-dominated regime (c.f. Fig. 6 (a)). However, there is an increasing asymmetry around $z = 0.5$ for higher modulation depths. A modulation depth dependent phase delay, as compared to the cosinusoidal intensity distribution, can be observed, namely the intersections with the bias voltage are shifted to the left for high modulation depth m. This delay gives rise to a modulation depth dependent phase of the correction function $f(m)$, as it will be discussed below. Furthermore, the situation in Fig. 7 can be compared with the results shown in Fig. 6 (c), because the applied field strength E_0 is the same and the intensity pattern is taken again at the starting position (c.f. Fig. 5). Obviously, the movement of the fringes leads to a totally different response of the crystal. Besides the sinusoidal, instead of cosinusoidal, shape of the electric field E, the maximum and the minimum of the electric field approximately exhibit the same distance from the bias voltage, another considerable difference to Fig. 6 (c).

Starting from the space charge field solutions presented above, we want to get a better insight into the nonlinear behavior of the first Fourier component. To determine a correction function based on the underlying KE, we solve Eq. (3) for the stationary state, when all transients have died away. This solution reads

$$Q = \frac{\Gamma}{2\left(\eta - \mathrm{i}\delta\omega\tau\right)} f(m) e^{\mathrm{i}(\psi_1 - \psi_2)}, \tag{18}$$

where the phase difference $\psi_1 - \psi_2$ is equal to $-\delta\omega t$ and an ansatz $Q(t) = Q_0 \exp\left[\mathrm{i}\left(-\delta\omega t\right)\right]$ has been used in Eq. (3). The frequency $\delta\omega$ is equal to 0 for static interference patterns, and $\delta\omega \neq 0$ corresponds to moving interference patterns.

Before determining the correction function, we interpret the physical meaning of Eq. (18) with respect to the results of the simulations on static and running gratings. The phase of Q is linearly influenced by the phase of the interference pattern $\psi_1 - \psi_2$. This linear phase response is consistent with the model of an infinitely extended crystal, which is exposed to a periodic intensity pattern. Evidently, in this situation a phase shift of the interference pattern causes a phase shift of the space charge field by the same amount, owing to the periodic boundary conditions. Analogously, a complex correction function $f(m)$, instead of a
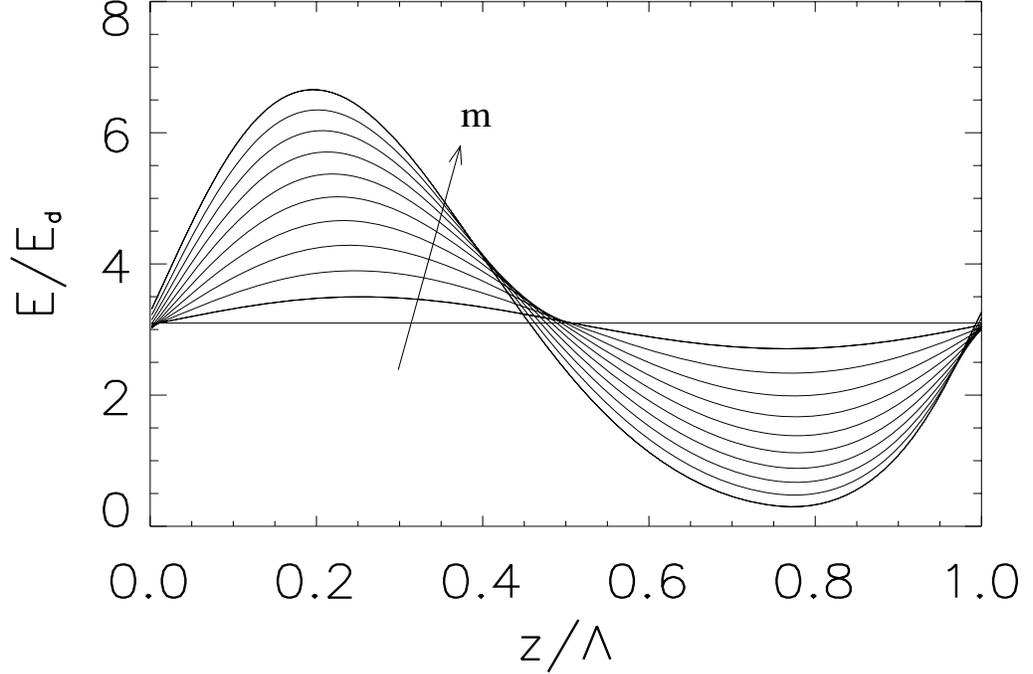
Figure 7: Total electric field in the crystal $E = E_0 + E^{\mathrm{sc}}$ for an applied external field of $E_0 = 3.1E_{\mathrm{d}}$ and an intensity pattern running with a frequency of $\varpi = 0.25$. The modulation depth is varied from $m = 0$ to $m = 1.0$ in steps of $\Delta m = 0.1$. The direction of increasing m is indicated by the arrow and the picture is taken at $t \approx 502.7\tau_{\mathrm{R}}$, corresponding to 20 temporal periods.

real function, physically corresponds to a modulation depth dependent phase shift of the space charge field.

The first Fourier component of the (scaled) space charge field $\widetilde{w}_1$ is, according to Eq. (18), proportional to $f(m)$ via the connection $\widetilde{w}_1 \propto E_1^{\mathrm{sc}} \propto Q$. Thus, the high-$m$ correction function can be determined via a simple scaling law:

$$f(m) = \frac{\widetilde{w}_1(m)}{\widetilde{w}_1(m_{\mathrm{s}})}m_{\mathrm{s}}. \tag{19}$$

Here m_{s} is a sufficiently small modulation depth, for which the analytical solution from the small modulation depth approximation holds. Therefore, $f(m)$ is computed by relating the first-order Fourier components of the space charge field for equal E_0, the same frequency $\varpi = \delta\omega/(\gamma_{\mathrm{R}}N_{\mathrm{A}})$ and identical phase difference of the interference pattern $(\psi_1 - \psi_2)$. The requirement for the identical phase difference implies that for running gratings the space charge field components $\widetilde{w}_1$ for the same times have to be used in Eq. (19). For extracting $f(m)$, we use $m_{\mathrm{s}} = 0.01$ as the small modulation depth. To be sure that the first Fourier component of the space charge field has converged into a stationary state, we multiply this quantity with a factor of $\exp(i\varpi t)$, to get rid of its fast time dependence (time scaled to τ_{R}). A temporally constant value of $\widetilde{w}_1 \exp(i\varpi t)$ indicates convergence.

The plot of the real part of $f(m)$ as a function of the modulation depth m, according to Eq. (19), is shown in Fig. 8 for static and running gratings. Additionally the (real) linear response $f(m) = m$ and the (real) sublinear and superlinear response $f(m) = m/(1 + bm)$ have been plotted. The curves for static intensity distributions are all the same, independent of the applied field strength E_0. The real part of the
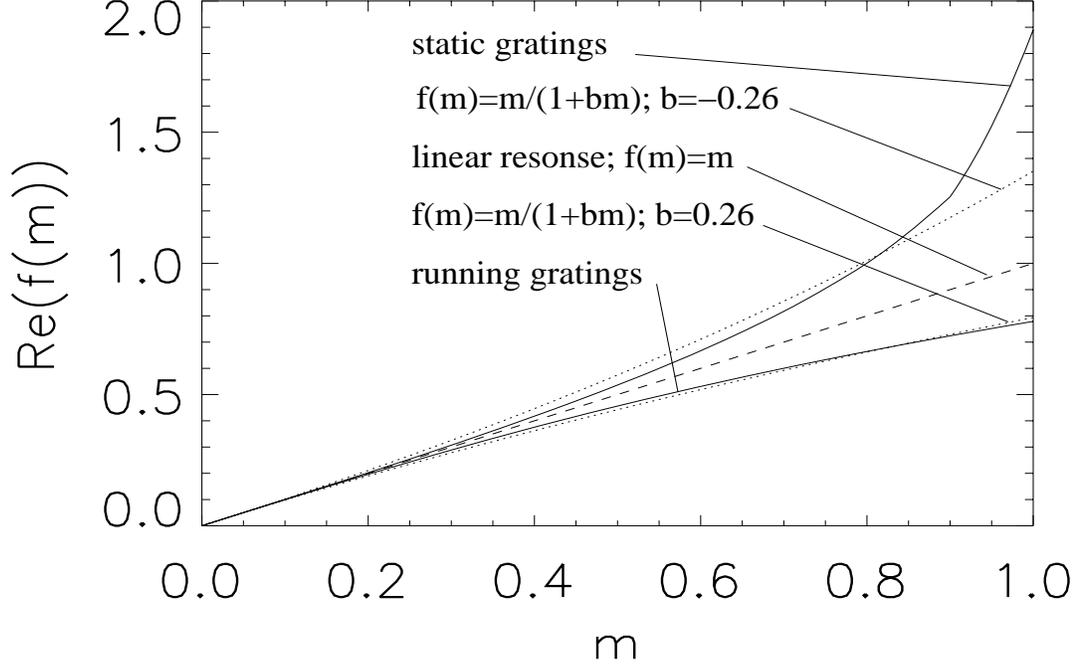
Figure 8: Real part of the physically motivated correction functions $f(m)$ as determined from exact simulations of the Kukhtarev equations. The response for the static and dynamic cases is indicated. Additionally the linear response $f(m) = m$ and $f(m) = m/(1 + bm)$ [4] are displayed.

correction function behaves superlinearly for static intensity patterns. However, the real part of $f(m)$ exhibits a sublinear response for a running grating ($\varpi = 0.25$ in this case). A saturation $b \approx 0.26$ fits the sublinear curve $\text{Re}(f(m))$ very well, whereas the value $b \approx -0.26$ fits the superlinear case. This behavior of the real part of $f(m)$ is analogous to the results in Refs. [8, 9], where it was demonstrated that for running intensity patterns, based on the KE, a sublinear response is obtained.

Owing to the complex coefficients $\widetilde{w}_1$ in Eq. (19), the modulation depth correction function $f(m)$ should generally be considered complex (see Fig. 9). Even in the complex plane the computed curves for static intensity distributions are identical, independent of the applied field strengths E_0. There is no numerically relevant imaginary component observed, so that the correction function is completely real. Hence, the non-linear response of the crystal is, in the static regime, fully described by a superlinear real correction function. This is in agreement with results given in Refs. [20, 23, 26] (for different crystal parameters), where the statement was made that the amplitude of the first Fourier component is larger than predicted by the small m approximation. However, for running gratings a pronounced imaginary part occurs. This fact is due to the modulation depth dependent phase shift shown in Fig. 7. To our knowledge, this effect has been reported for the first time by us, in [18]. The majority of papers published on TWM only discuss effects related to intensities, such as gain, etc. Phase effects in TWM are mostly ignored, and with them also the modulation depth dependent phase shift for dynamic gratings. For running gratings a complex correction function

$$f(m) = |f(m)| e^{i\varphi(m)} \tag{20}$$

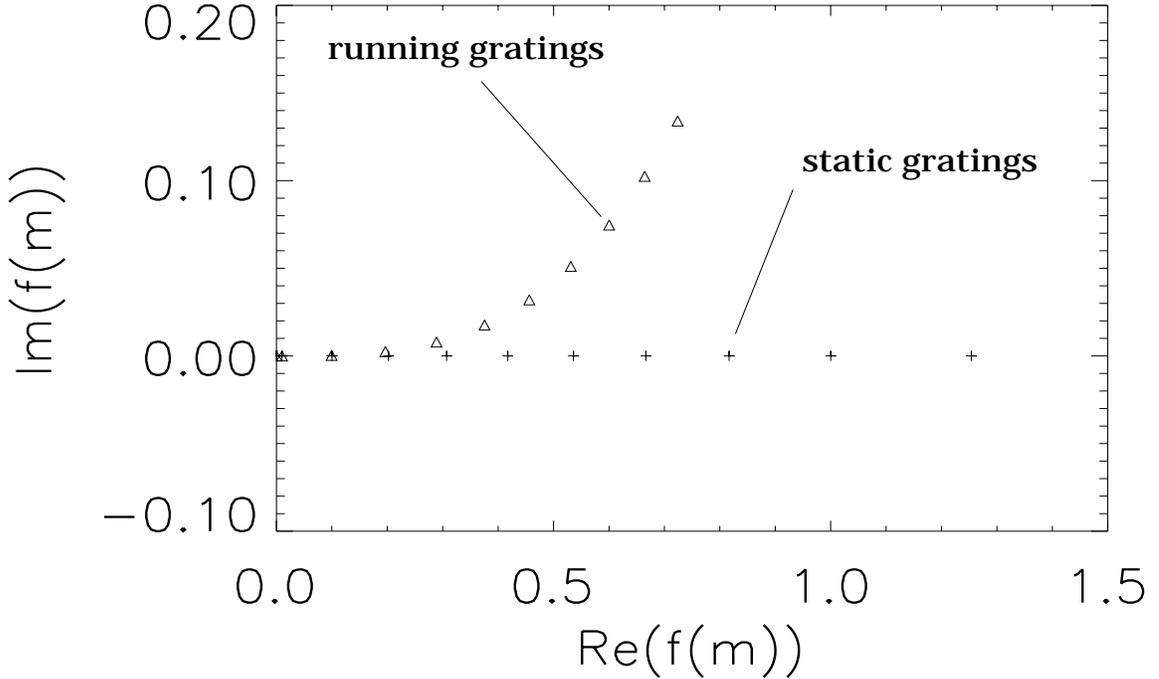is required for a more realistic description of a PR crystal.

Figure 9: Real and imaginary parts of the computed modulation-depth-dependent correction function $f(m)$ for $(+)$ static and $(\triangle)$ running gratings. The modulation depth has been varied from $m = 0$ to $m = 0.9$ in steps of $\Delta m = 0.1$.

4. Conclusions

The influence of a high modulation depth on pattern formation and the foundation of the high modulation depth correction function are discussed. The results from numerical simulations of TWM for Gaussian beams are found to be in good agreement with the critical quantities predicted by the linear stability analysis.

The influence of high saturation on the pattern formation shows up in an increase of the critical electric field strength and a stronger critical detuning of the side-band beams. As a characteristic feature of the onset of patterns, a modulation depth close to unity is required at the side of the crystal where the pump beam enters. Even for small signal and high pump beam intensities, transverse patterns arise if the external field strength is adjusted in such a way that a modulation depth of about one is achieved. Therefore, effects of high modulation depth have to be considered when pattern formation in the contra-directional configuration is discussed.

Compared to the case of linear response [16], besides transverse running waves, no qualitatively new patterns are observed near and above the instability threshold. Independent of the saturation, the simulations show periodic, symmetric beam profiles. Quantitatively, however, a stronger sublinear response of the crystal leads to a stronger detuning of the side-band beams, and the pattern amplitude increases more slowly with respect to the applied field strength. The simulations of the TWM equations show that the gain, i. e. the amplification of the signal beam, saturates above the instability threshold. Pattern formation therefore prevents a further enhancement of the signal.

The physical foundation of the high modulation depth corrections are also discussed. In an attempt to justify the presumed form of the correction functions, used in Refs. [3, 4] to explain experimental results, a new spectral integration scheme is developed to accurately solve KE.

The response of the space charge field to static and running intensity distributions is explored for different applied external electric fields. Phase shifts due to the external field are demonstrated, together with the transition from the diffusion-dominated crystal response to the drift-dominated regime. These observations motivate a superlinear response of the investigated BSO crystal for stationary intensity distributions. Recently a superlinear behavior has been observed in experiments on TWM in a $KNbO_3$ crystal [27]. This substantiates our finding that the sublinear correction function proposed by Kwak [4] for static gratings is not appropriate, and that one should utilize negative saturations in this regime. For running gratings complex correction functions (with a sublinear real part) are necessary, to take properly the modulation depth effects into account.

References

[1] N. V. Kukhtarev, V. B. Markov, S. G. Odulov, M. S. Soskin, V. L. Vinetskii, Ferroelectrics 22 (1979) 949.

[2] P. Yeh, Introduction to Photorefractive Nonlinear Optics, Wiley & Sons, New York, 1993.

[3] Ph. Refregier, L. Solymar, H. Rajbenbach, J.P. Huignard, J. Appl. Phys. 58 (1985) 45.

[4] C. H. Kwak, S. Y. Park, J. S. Jeong, H. H. Suh, E. Lee, Opt. Comm. 105 (1994) 353.

[5] V. Dupray, M. Brunel, C. Özkul, N. Wolffer, J. Opt. Soc. Am. B 17 (2000) 407.

[6] J. E. Millerd, E. M. Garmire, M. B. Klein, B. A. Wechsler, F. P. Strohkendl, J. Opt. Soc. Am. B 9 (1992) 1449.

[7] M. R. Belić, D. Timotijević, M. Petrović, M. V. Jarić, Opt. Comm. 123 (1996) 201.

[8] L. B. Au and L. Solymar, Opt. Lett. 13 (1988) 660.

[9] G. A. Brost, K. M. Magde, J. J. Larkin, M. T. Harris, J. Opt. Soc. Am. B 11 (1994) 1764.

[10] T. Honda, Opt. Lett. 18 (1993) 598; 20 (1995) 851.

[11] P. P. Banerjee, H.-L. Yu, D. A. Gregory, N. Kukhtarev, H. J. Claufeld, Opt. Lett. 20 (1995) 10.

[12] M. Schwab, M. Sedlatschek, B. Thüring, C. Denz, T. Tschudi, Chaos Solitons Fractals 10 (1998) 701.

[13] C. Denz, M. Schwab, M. Sedlatschek, T. Tschudi, T. Honda, J. Opt. Soc. Am. B 15 (1998) 2057-2064

[14] M. Saffman, D. Montgomery, A. A. Zozulya, D. Z. Anderson, J. Opt. Soc. Am. B 11 (1994) 1409.

[15] T. Honda and P. P. Banerjee, Opt. Lett. 21 (1996) 779.

[16] O. Sandfuchs, F. Kaiser, M. R. Belić, J. Opt. Soc. Am. B 15 (1998) 2070.

[17] O. Sandfuchs, F. Kaiser, M. R. Belić, Phys. Rev. A 64 (2001) 063809.

[18] F. Pauly, O. Sandfuchs, F. Kaiser, M. R. Belić, Opt. Commun. 218 (2003) 385.

[19] N. Singh, S. P. Nadar, P. P. Banerjee, Opt. Comm. 136 (1994) 487.

[20] G. A. Brost, J. Opt. Soc. Am. B 9 (1992) 1454.

[21] Y. H. Lee and R. W. Hellwarth, J. Appl. Phys. 71 (1992) 916.

[22] P. Buchhave, J. Opt. Soc Am. B 15 (1998) 1865.

[23] E. Serrano, V. López, M. Carrascosa, F. Agulló-López, IEEE J. Quant. Electron. 30 (1994) 875.

[24] F. Vachs and L. Hesselink, J. Opt. Soc. Am. A 5 (1988) 690.

[25] N. V. Kukhtarev, P. Buchhave, S. F. Lyuksyutov, Phys. Rev. A 55 (1997) 3133.

[26] A. Bledowski, J. Otten, K. H. Ringhofer, Opt. Lett. 16 (1991) 672.

[27] D. Tamer, Diploma thesis, Darmstadt University of Technology, 2000.